Australian Journal of Earth Sciences
Publication details, including instructions for authors and subscription information:
http://www.informaworld.com/smpp/title~content=t716100753

Mineralogy of gouge in north-northeast-striking faults, Sydney region, New South Wales

R. Offler [a]; D. J. Och [b]; D. Phelan [c]; H. Zwingmann [d]
[a] Discipline of Earth Sciences, School of Environmental & Life Sciences, University of Newcastle, NSW, Australia [b] New South Wales Department of Primary Industries, Londonderry, NSW, Australia [c] EM/X-Ray Unit, University of Newcastle, NSW, Australia [d] CSIRO Petroleum, Bentley, WA, Australia

Online Publication Date: 01 October 2009

To cite this Article Offler, R., Och, D. J., Phelan, D. and Zwingmann, H.(2009)'Mineralogy of gouge in north-northeast-striking faults, Sydney region, New South Wales',Australian Journal of Earth Sciences,56:7,889 — 905
To link to this Article: DOI: 10.1080/08120090903005352
URL: http://dx.doi.org/10.1080/08120090903005352

Australian Journal of Earth Sciences (2009) **56**, (889–905)

Mineralogy of gouge in north-northeast-striking faults, Sydney region, New South Wales

R. OFFLER[1]*, D. J. OCH[2], D. PHELAN[3] AND H. ZWINGMANN[4]

[1]*Discipline of Earth Sciences, School of Environmental & Life Sciences, University of Newcastle, NSW 2308, Australia.*
[2]*New South Wales Department of Primary Industries, Geological Survey of New South Wales, Londonderry, NSW 2753, Australia.*
[3]*EM/X-Ray Unit, University of Newcastle, NSW 2308, Australia.*
[4]*CSIRO Petroleum, PO 1130, Bentley, WA 6102, Australia.*

Gouges formed in north-northeast-striking fault zones of the Sydney region and associated host-rocks were investigated by XRD, SEM, TEM and optical microscopy in order to determine their mineralogy. XRD studies reveal that illite, illite–smectite, kaolinite, quartz and dickite are present in varying proportions. Kübler Indices (0.54–0.71) and low smectite contents in illite–smectite (< 10% smectite) in most gouges and host-rocks, indicate the assemblages formed at temperatures between 120 and 150°C. Those at the Heathcote Road, Lucas Heights location formed at lower temperatures (< 100°C). SEM images of the clays in host sublitharenites and gouges show a variety of sizes and habits that reflect variations in fluid temperature and rate of crystallisation. SEM studies also reveal that detrital quartz grains exhibit overgrowths and etch pits of varying density, size and shape that are more strongly developed in the gouges than in the host-rocks. These features are thought to be related to higher fluid/rock ratios brought about by major ingress of fluids into the fault zones. The mineral assemblage present and the features exhibited are believed to have formed in response to a thermal event associated with the early stages of the breakup of Gondwana.

KEY WORDS: faults, gouge, mineralogy, Sydney region.

INTRODUCTION

Structural studies in the Sydney region have revealed the presence of major north-northeast-striking faults in the Triassic Narrabeen Group, Hawkesbury Sandstone and Wianamatta Group (Figure 1) (Och *et al.* 2009). K–Ar dating of illite and illite–smectite in fractions extracted from gouges developed in these faults shows ages varying from 148 to 115 Ma in the coarser fractions (0.5–1.0 to 2–10 μm: mean 131 Ma) and 138 to 107 Ma in the finest fractions (< 0.1–0.5 μm: mean 121 Ma). The dates obtained from the finer fractions are thought to record a thermal event associated with felsic intrusions emplaced during the early stages of the breakup of Gondwana (Och *et al.* 2009).

To complement these studies, a petrographic examination has been conducted on host-rocks outside and within the fault zones, and X-ray diffraction (XRD) analyses have been carried out on fractions previously dated by the K–Ar technique to determine their mineralogy, the presence of mica polytypes, the crystallinity of illite (Kübler Index) and the temperature at which the mineral assemblages formed. Backscatter scanning electron microscope (BSEM), energy dispersive spectrometry (EDS) and transmission electron microscopic (TEM) studies of gouges and associated host-rocks have also been carried out to ascertain the morphology and composition of the mineral phases in the host-rocks and gouges, in order to determine the conditions prevailing during deformation. The outcomes of this study are reported here and the associated data are compared with those reported by other authors for the Late Permian–Early Triassic rocks in the Sydney Basin (Bayliss *et al.* 1965; Bai & Keene 1996; Bai *et al.* 2001).

TECHNIQUES

Samples previously prepared for K–Ar analysis (Figure 1; Table 1) (Och *et al.* 2009) were investigated by XRD and SEM (University of Newcastle) and TEM (Curtin University of Technology, Perth).

X-ray diffraction

XRD patterns were obtained using a Philips automated PW1732/10 X-ray diffractometer, with CuK(radiation, graphite monochromator and operating conditions of 40 kV/30 Ma.

Kübler Indices

Fractions of < 2 μm were separated from whole-rock powders in distilled water according to Stokes' Law. To maintain a constant thickness, ~3 mg/cm of sediment

*Corresponding author: robin.offler@newcastle.edu.au

ISSN 0812-0099 print/ISSN 1440-0952 online © 2009 Australian Government
DOI: 10.1080/08120090903005352

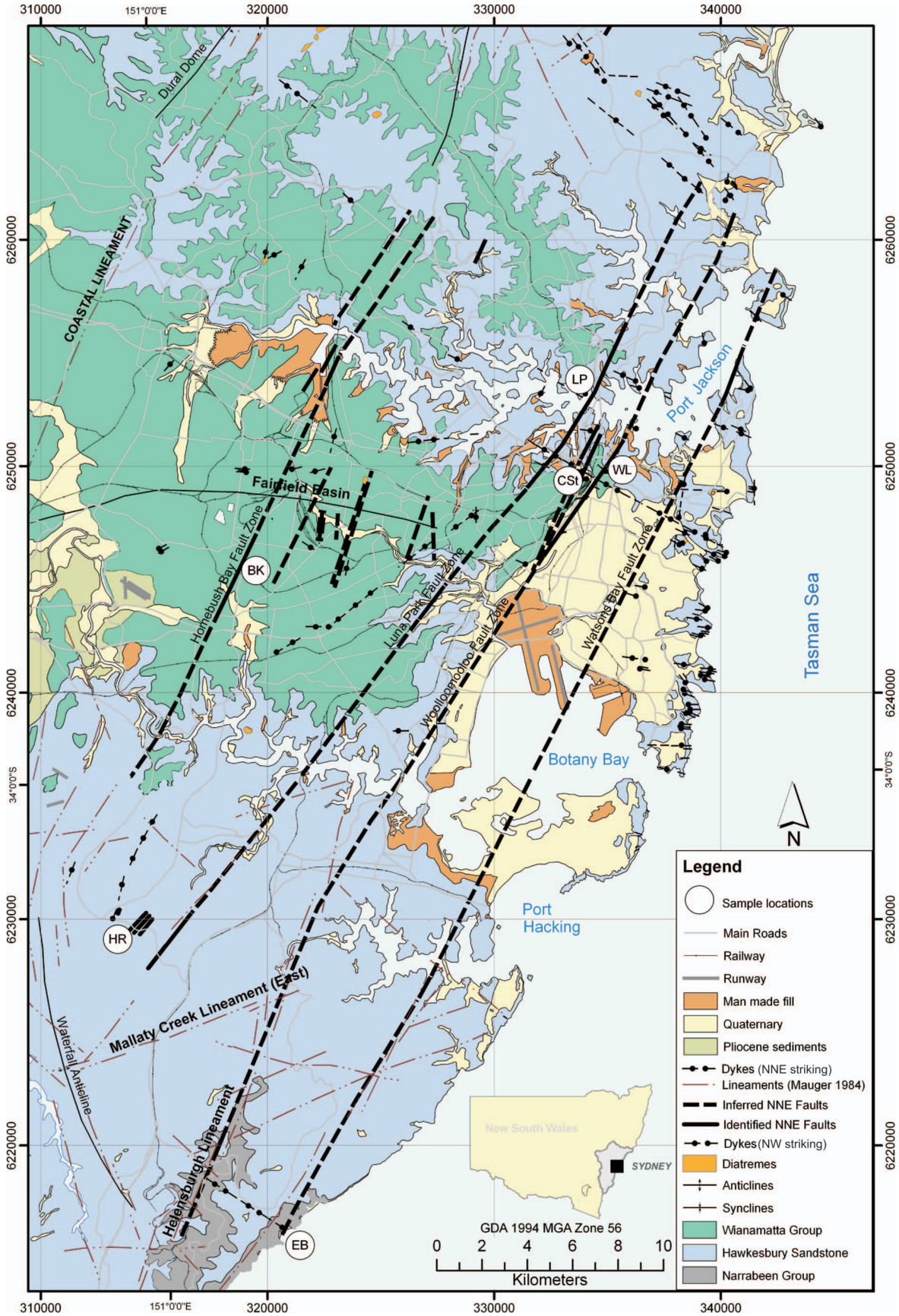

Figure 1 Simplified geology map of the study area showing location of main north-northeast-striking fault zones, dykes and sample locations (after Herbert 1983; Mauger *et al.* 1984; Stroud *et al.* 1985; Clark & Jones 1991). LP, Luna Park; WL, Woolloomooloo cross-city tunnel east; HR, Heathcote Road; CSt, Cunningham Street; EB, South Era Beach; BK, Bankstown.

Table 1 Mineral phases in each fraction (air-dried).

Sample no.	Location	Coordinates[a]		2–6 μm	<2 μm	<0.4 μm			% I in I/S-<2 μm	% I in I/S-<0.4 μm
		Easting	Northing							
Gouge										
630[b]	Heathcote Road Fault Zone (HR)	314210	6229524	K-(I/S)-(H),	H-K-(I/S)-(I)	H-K-(I/S)-(I)			70	69
631	Heathcote Road Fault Zone (HR)	314210	6229524	(I/S)-K-(I)	I/S-K-H-I-Q				68	–
632	Heathcote Road Fault Zone (HR)	314210	6229524	K-I/S-I	I/S-I-(K)	I/S-I-(K)			66	62
633	Heathcote Road Fault Zone (HR)	314210	6229524	H-I/S	K-I/S-(I)				69	–
				2–10 μm	<2 μm	1–2 μm	1–0.5 μm	<0.5 μm	<2 μm	
LP1	Luna Park Fault Zone (LP)	334461	6253153	–	Q-K-I-(1Mt)[c]	Q-K-(I)-(D)-(1Mt)	Q-I-(K)-(1Mt)	Q-I-(K)-1Mt	>90	
LP2	Luna Park Fault Zone (LP)	334461	6253153	–	Q-K-I	–	–	–	>90	
LP3	Luna Park Fault Zone (LP)	334461	6253153	K-D-Q-I	Q-K-I	Q-K-(D)-(I)-1Mt	–	Q-I-(K)-1Mt	>90	
LP4	Luna Park Fault Zone (LP)	334461	6253153	–	Q-K-I	–	–	–	>90	
LP5	Luna Park Fault Zone (LP)	334461	6253153	–	K-I/S-Q	–	–	–	>90	
LP6	Luna Park Fault Zone (LP)	334461	6253153	–	I-Q-(K)	–	–	–	>90	
599	Woolloomooloo Fault Zone (WL)	335184	6250331	–	I-Q-(K)	–	–	–	>90	
671	Luna Park Fault Zone (LP)	334461	6253153	–	K-I/S-I-Q	–	–	–	>90	
306	Watsons Bay Fault Zone (EB)	320674	6216113	–	C/S-I/S-K	–	–	–	>90	
Host										
709	Cunningham Sreet (CSt)	334144	6249872	–	K-I/S-I-Q	–	–	–	>90	
LPC2	Luna Park (LP)	334461	6253153	–	K-I/S-I-Q	–	–	–	>90	

[a]AGD 1994 MGA Zone 56.
[b]TEM/SEM shows halloysite present.
[c]>2 μm.
K, kaolinite; Q, quartz; D, dickite; I, illite; 1Mt, mica polytype; I/S, illite–smectite; C/S, chlorite–smectite; H, halloysite.

was pipetted onto each slide. In this way variation in intensity and peak width caused by variation in sediment thickness could be avoided (Krumm & Buggisch 1991; Kisch 1991). Samples were scanned over the range $2\theta = 6.5$–10° at 0.5° 2θ/min using divergence slits of 1° and receiving slits of 0.1 mm. 'Illite Crystallinity' [(IC): Kübler 1968; now referred to as the Kübler Index (KI): Guggenheim *et al.* 2002] was determined from the width of the (001) peak at half-peak height and expressed in terms of $\Delta 2\theta$ (Kisch 1991). KI values were then converted to CIS (Crystallinity Index Standard) values (Warr & Rice 1994) using calibration curves based on standards provided by L. N. Warr. Following Warr & Rice (1994), values indicate epizonal conditions if KI = 0.25 or less, anchizonal if $0.25 < \mathrm{KI} < 0.42$ and diagenetic if $\mathrm{KI} > 0.42$. Glycolation was required to obtain true KI values because the (001) peaks were asymmetrical in some samples due to the presence of illite–smectite. Deconvolution of these peaks was also carried out using the Philips ProFit program to determine KI values.

Mineral identification

Fractions separated from the samples were sedimented by pipette onto glass slides and packed into mounts designed by Robinson (1981) for the determination of the mineralogy and polytypes. Diffractograms were acquired from air-dried, glycolated and heated (550°C) slides and analysed by XRD using the same equipment as for the KI. Samples were scanned over the range $2\theta = 2$–30° at 0.02° 2θ/s using divergence and scatter slits of 1° and a receiving slit of 0.2 mm. Identification of clay mineralogy and determination of the percentage of illite in illite–smectite were carried out following the methods of Moore & Reynolds (1997). Identification of mica polytypes was based on the peak positions and Miller Indices reported by Drits *et al.* (1993) and Lanson *et al.* (1996); kaolin-group minerals were identified using the diagnostic peaks suggested by Beaufort *et al.* (1998) and Lanson *et al.* (2002). The presence of halloysite, first recognised in reconnaissance TEM studies, was difficult to establish because of the occurrence of kaolinite and other phases in the various fractions. Confirmation was based on the (02,11) reflection at d = 4.46 Å and other less well-developed diagnostic reflections (Bailey 1980).

Scanning electron microscopy

Scanning electron microscope (SEM) images were obtained from a PHILIPS XL30 SEM to determine the morphological features and size of the white mica and kaolinite plates exposed in samples that had been broken approximately perpendicular to bedding. Additionally, SEM studies were carried out on detrital quartz grains separated out from gouges and host-rocks to ascertain whether dissolution had occurred during diagenesis or during fluid movement through the fault zones. Back scatter electron images were obtained from polished thin sections.

Transmission electron microscopy

A JEOL JEM 2010 200KV TEM at Curtin University was used for a detailed grain-by-grain characterisation of the <0.5 μm and <2 μm clay mineral fractions from several samples (545, 549; Luna Park Fault Zone; 599; Woolloomooloo Fault Zone; 630, 631; Heathcote Road Fault Zone: Table 1). Clay particle morphologies were investigated as well as the grainsize distribution within the fractions. One drop of clay solution was loaded on a micro carbon grid film and dried under air. Composition of individual particles was investigated by an attached EDS system.

RESULTS

Petrography of host-rocks within and external to fault zones

The host-rocks distant from the Luna Park Fault Zone (LP in Figure 1) are sublitharenites consisting of slightly elongate, subangular to angular detrital quartz (0.15–0.28 mm length; 0.7–0.14 mm width; ~70% modal volume) and minor detrital muscovite (~5%). Grainsize patches of illite and kaolinite occur, as well as isolated aggregates of siderite (~5%) that are often concentrated on bedding planes in association with opaque minerals and detrital muscovite.

Both the quartz and muscovite show varying degrees of internal strain, manifested as moderately developed undulose extinction or as deformation lamellae in the former and as kinking, bending and folding in the latter. Corrosion of quartz associated with the minerals filling pore spaces is a feature, and overgrowths are uncommon. Suturing of boundaries between quartz grains is also common. In the pore spaces and wrapping around the quartz are aggregates of illite and kaolinite (~20%; illite >> kaolinite). Accessory minerals comprise zircon, irregular opaque minerals (e.g. anatase) and very minor tourmaline and sphalerite.

Samples within the damage zone and gouges of the Luna Park Fault Zone have a similar mineralogy, but the proportion of clays is lower. Corrosion of detrital quartz is also greater and quartz overgrowths are very common (Figure 2a, c, d). In some samples, the overgrowths may be corroded when in contact with kaolinite and illite, in others kaolinite formation appears to be synchronous with overgrowth formation (Figure 3c). Replacement of detrital muscovite by very fine-grained aggregates of illite and kaolinite is also a feature (Figure 2b).

Host-rocks adjacent to and within other fault zones generally show similar mineralogy and textures. However, illite may be a more common phase in pore spaces and proportionally higher in samples adjacent to the fault zones. (e.g. 631; Heathcote Road Fault Zone; up to 20%: HR in Figure 1). Other observations include the lack of overgrowths on most quartz grains in sublitharenite fragments associated with gouge from the Heathcote Road Fault Zone, and grain-boundary suturing in sublitharenites from the Woolloomooloo Fault Zone (WL in Figure 1). Chlorite is an additional phase in litharenites of the Narrabeen Group at South Era Beach (EB in Figure 1). The significance of these observations will be discussed later.

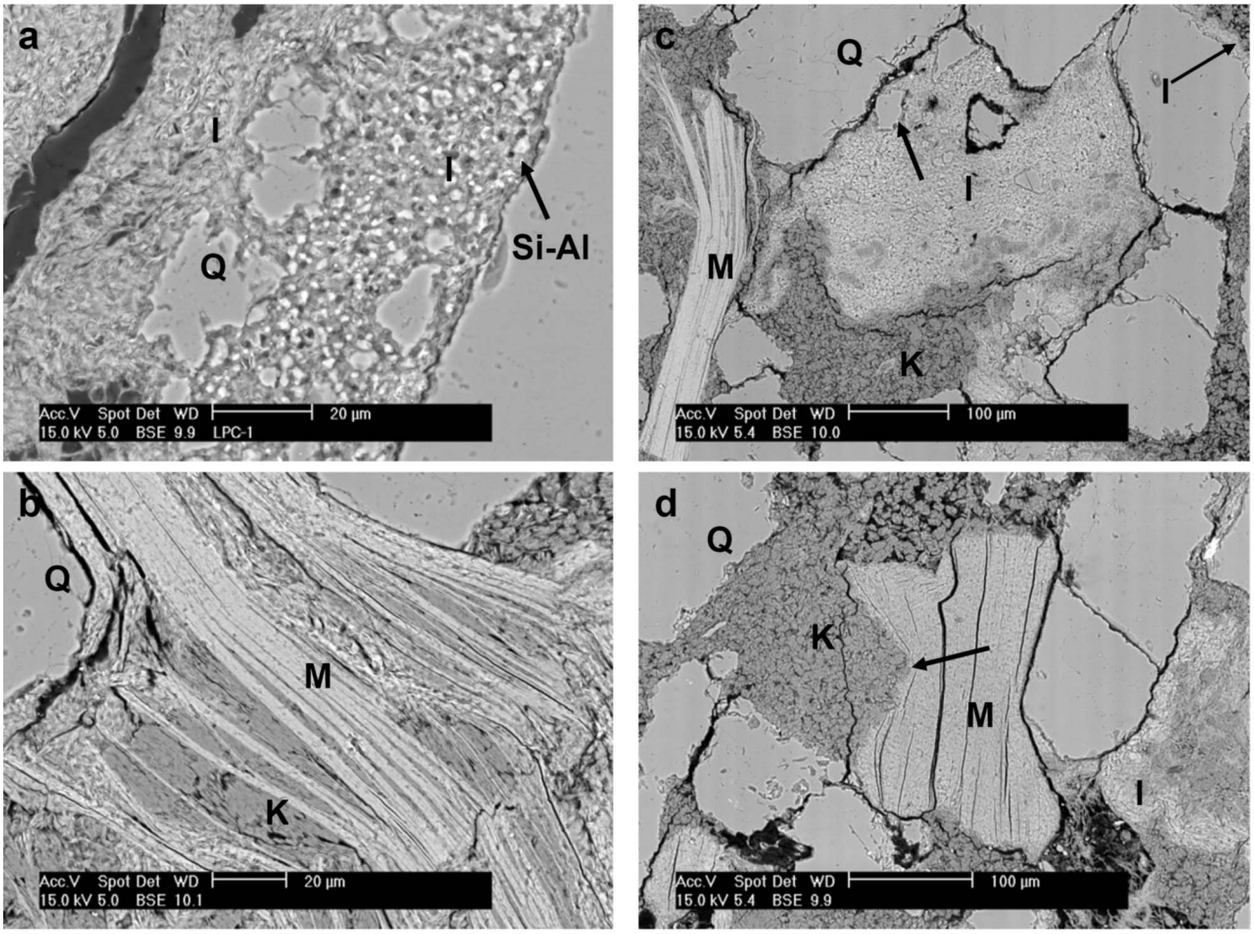

Figure 2 (a) Reaction front made up of relict 'islands' of extensively corroded quartz (Q), illite aggregates (I) and small, residual, Si-rich, Al-poor 'islands' (white; Si-Al) between illite (I) and detrital quartz: sublitharenite (LPC-1) from the damage zone of Luna Park Fault Zone. (b) Kaolinite (K) and illite (I) replacing detrital muscovite (M) along the (001) cleavage: LPC-1. (c) Kaolinite (K) and illite (I) aggregates associated with detrital quartz (Q) and muscovite (M). Note corroded boundaries of quartz (arrow): LPC-1. (d) Indentation of detrital muscovite (M) by feldspar? replaced by kaolinite aggregates (K). Illite aggregates (I) are associated with kaolinite aggregates (K), right-hand side of image LPC-1. All samples are stored in the School of Environmental & Life Sciences, University of Newcastle.

Mineralogy and crystallinity

XRD studies of various fractions from gouges reveal that illite, illite–smectite [<10% smectite (Sme)—mineral abbreviation from Siivola & Schmid 2007], kaolinite, quartz, chlorite, dickite and halloysite are present in varying proportions (Figures 4–6; Table 1). Halloysite is a major phase in most samples from the Heathcote Road Fault Zone, and is associated with illite–smectite (30–38% Sme; Table 1; Figure 5). 1Mt mica polytype occurs in gouge from the Luna Park Fault Zone (Figures 4, 6), particularly in the finer fractions. Dickite, on the other hand, is only present in the coarse fractions from this fault zone (Figure 6). Anatase is an accessory in samples 630, 631 (Heathcote Road Fault Zone) and 545 (Luna Park Fault Zone). KI obtained from illite in <2 μm fractions are variable, but overall they indicate that the illites are thermally immature and have formed under diagenetic conditions (Table 2). The <2 μm fractions extracted from the sublitharenites have a similar mineralogy, consisting of illite/smectite (<10% Sme), kaolinite and quartz.

Clay morphology

SEM images of the clays exposed in the faces of broken samples outside and within the fault zones show kaolinite as pseudohexagonal plates, books, vermiform aggregates (LP6; LPC-1–Luna Park Fault Zone: Figure 7e) and ragged, poorly formed, curved, thin plates with irregular boundaries (LP6; LPC-2–Luna Park Fault Zone: Figure 7d). Blocky crystals of dickite are associated with kaolinite in some samples, and form an association similar to that reported by Lanson *et al.* (2002). Halloysite is also present in some gouges from the Heathcote Road Fault Zone, occurring as clusters of thin tubular or fibrous particles (0.7–1 μm long; 0.1 μm wide) hosted by quartz exhibiting etch pits (Figure 7f). Illite and illite/smectite occur as filamentous aggregates (LPC-2, LP3; LPC-3—Luna Park Fault Zone: Figures 3d, 7b) and more commonly as lath-like crystals, particularly in the gouge from the Luna Park Fault Zone. Filamentous growth appears to have occurred after the formation of the coarser kaolinite and illite, as fibrous illite occurs at the edges of these minerals (Figure 7b). However, in some

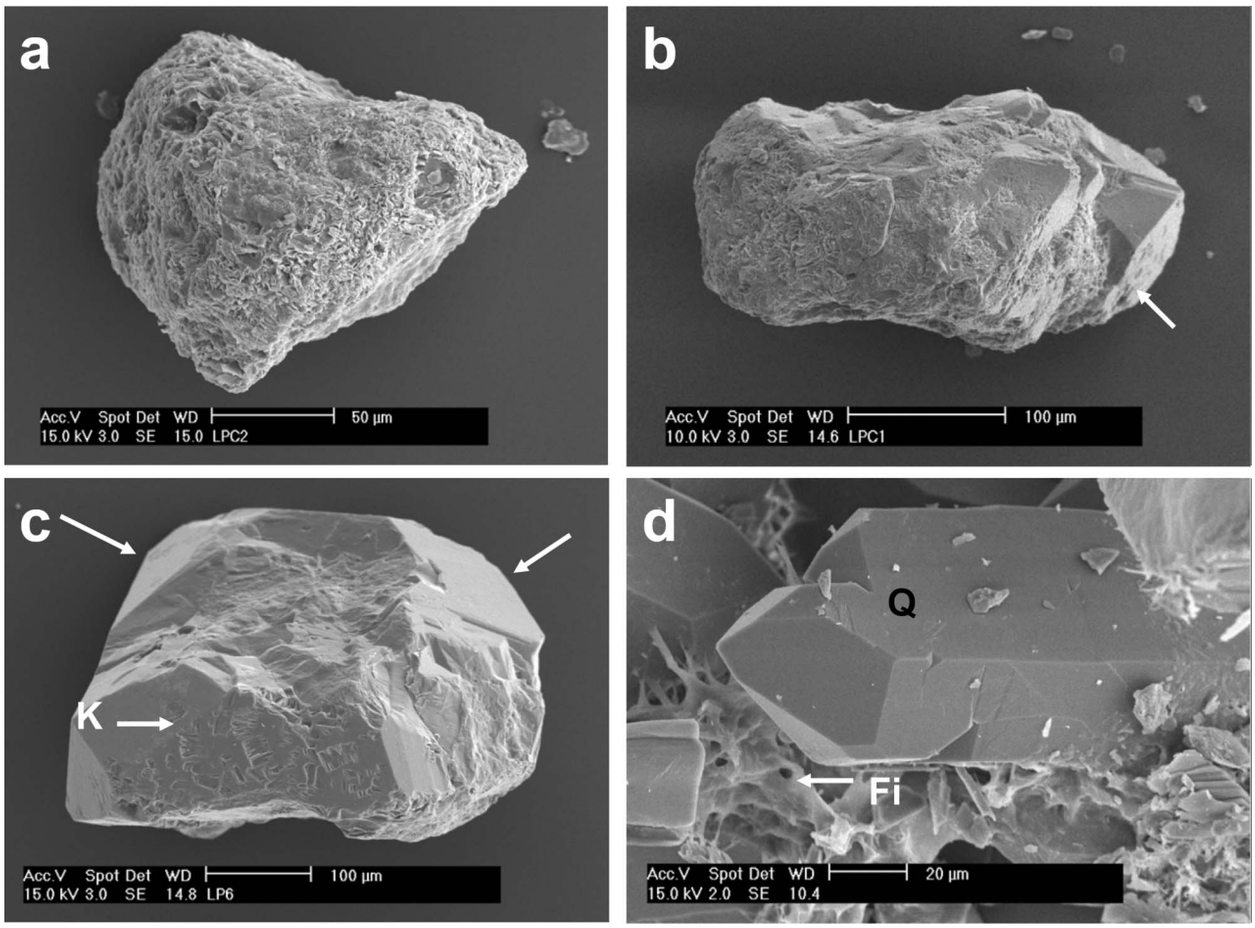

Figure 3 (a) Detrital quartz grain from sublitharenite (LPC-2) outside damage zone coated with fine grained, platy illite. (b) Detrital quartz grain from sublitharenite (LPC-1) in damage zone showing moderate overgrowth of quartz (arrow). (c) Detrital quartz grain from sublitharenite (LP6) in gouge exhibiting substantial quartz overgrowth (arrow) as well as negative crystal images of kaolinite books (K). (d) Euhedral quartz (Q) associated with filamentous illite (Fi) in sublitharenite (LP3) taken from gouge. All samples are stored in the School of Environmental & Life Sciences, University of Newcastle.

samples the fibrous illite appears to have grown synchronously with quartz overgrowths (Figure 3d).

SEM studies of polished thin-sections obtained from sublitharenites outside and within the damage zone and from gouges, show that in a few samples illite has grown prior to the development of quartz overgrowths and that fluids responsible for the growth of illite and kaolinite, extensively corrode detrital quartz and the overgrowths. Expansion and/or extensive replacement of muscovite by kaolinite along basal (001) planes has been noted in some samples and is a common feature observed in sandstones worldwide (Figure 2b) (Milliken 2003 and references therein). In rare instances, a zone containing grains of extensively corroded quartz, very fine-grained aggregates of illite and very small (1–2 μm), irregular, isolated Si-rich, Al and K-poor 'atolls' occurs between detrital quartz and fine-grained aggregates of illite (Figure 2a). An additional observation is the association of illite and anatase in grainsize patches. These appear to have replaced detrital biotite.

TEM observations of the clay fractions reveal two distinct groups of idiomorphic illite particles, namely fibres with elongated well-crystallised grain edges, and platy lath-like flakes (Figure 8b), together with hexagonal idiomorphic kaolinite with clear crystallised edges. All fractions contain minor amounts of quartz and Ti-rich mineral phases (anatase?). Also present in samples from the Heathcote Road Fault Zone is halloysite (Figure 8a) showing a characteristic tubular shape similar to that illustrated by Sudo *et al.* (1981).

Overgrowths and dissolution features of quartz

SEM studies show that detrital quartz in both the gouge and host-rocks exhibits overgrowths and dissolution (etch) pits of varying density, size and shape (Figure 9). The overgrowths are manifested as euhedral crystals attached to the detrital quartz grains, and are associated with neocrystalline kaolinite in samples from gouges (Figure 3c). Overgrowths are better developed in the gouges than in the host-rocks, and are a common feature of samples from the Hawkesbury Sandstone in the study area and in the underlying Narrabeen Group throughout the Sydney Basin (Bayliss *et al.* 1965; Bai & Keene 1996), particularly in the Sydney region that has been affected by the thermal overprint (Och *et al.* 2009). The pits occur on the surface of detrital quartz grains and on quartz overgrowths in most gouges and host rocks. They

Table 2 Kübler Index values.

Sample no.	Location	KI	KI (glyc)	KI (deconv.)
Gouge				
LP1	Luna Park (LP)	0.75	0.55	0.56[a]
LP2	Luna Park (LP)	–	0.56 (0.54)	–
LP3	Luna Park (LP)	0.82	0.71	0.54[b]
LP4	Luna Park (LP)	0.64	0.6 (0.57)	–
LP5	Luna Park (LP)	0.59	0.5 (0.55)	–
LP6	Luna Park (LP)	0.64 (0.61)	–	0.55[a]
599–2	Luna Park (LP)	0.76 (0.82)	0.67	–
Host				
709–2	CSt–Cunningham Street (CSt)	0.77	0.61	–
LPC-2	Luna Park (LP)	0.76	0.59	–
LPC-1	Luna Park (LP)	0.7	0.7	–

[a]Two peaks overlap with main peak.
[b]Three peaks overlap with main peak.
Numbers in parentheses [e.g. (0.54)] are repeat measurements.

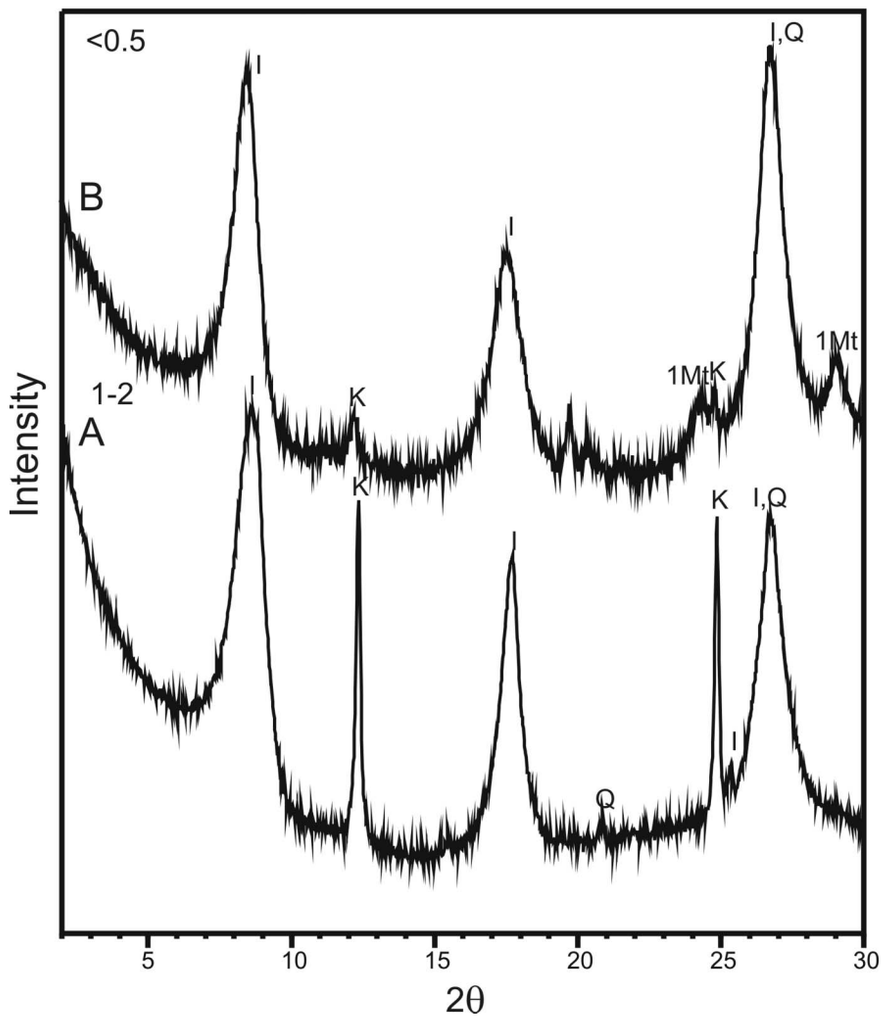

Figure 4 Air-dried XRD traces of LP3: A, 1–2 μm fraction; B, <0.5 μm fraction. Symbols as in Figure 2; Mt, mica polytype.

have triangular, cusp and rectangular shapes (Figure 9a). Further, they are commonly aligned and may be associated with well-developed prismatic surfaces and terraces (Figure 9b, e). They also occur as elongate trenches (5–10 μm long) oriented in varying directions and as irregular depressions; negative crystal shapes are common (Figure 9c). A consistent observation is that the pits appear to be preferentially developed on hexagonal prism faces of quartz in the overgrowths, a feature noted previously in phyllonites by Hippert (1994).

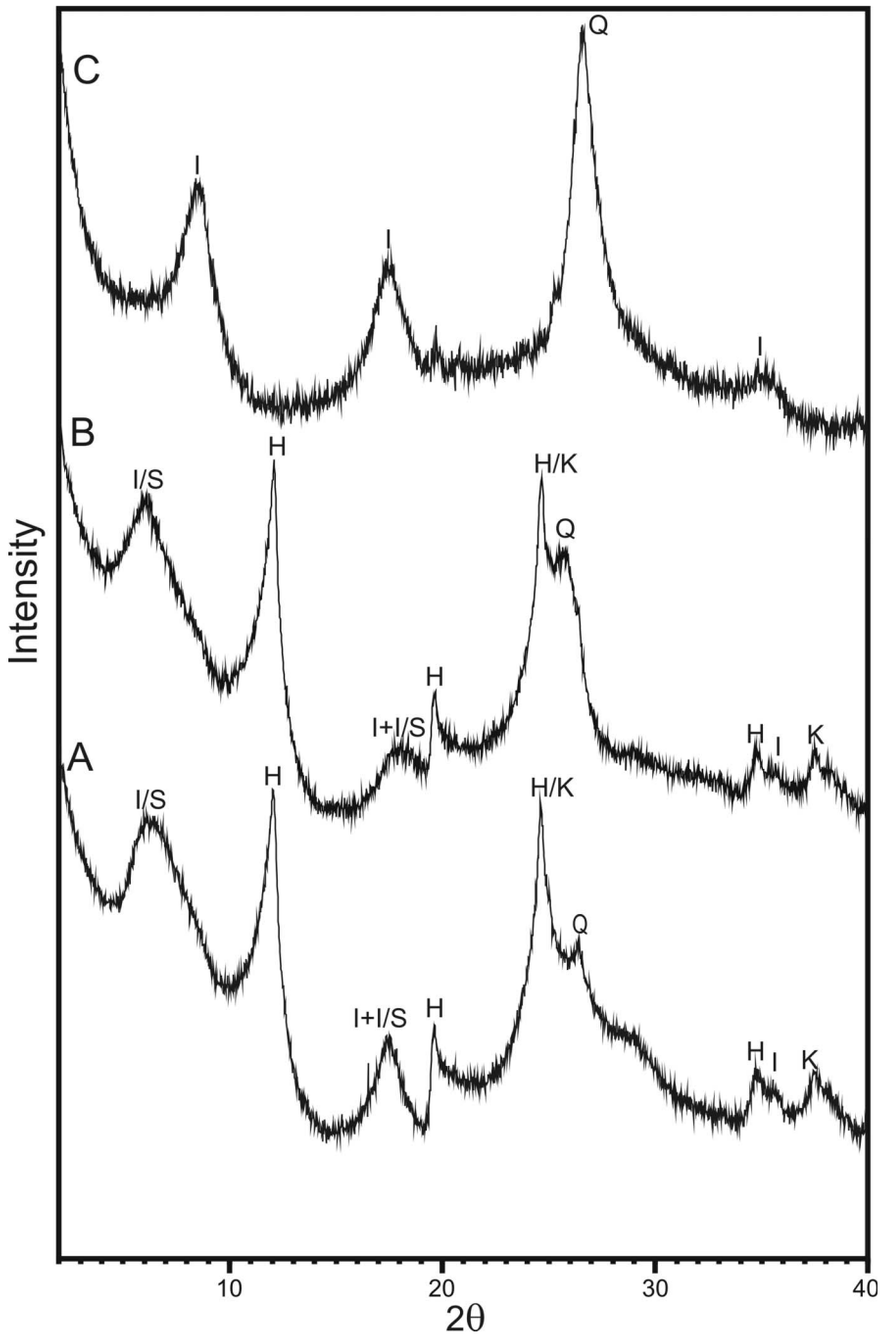

Figure 5 XRD traces of $<2\ \mu$m fraction of Sample 631 from the Heathcote Road Fault Zone: A, air-dried; B, glycolated; C, glycolated and heated (550°C). I, illite; H, halloysite; Q, quartz; I/S, illite–smectite.

Composition

The composition of detrital muscovite, illite and white mica with a bladed habit in the gouges, and sublitharenites outside (LPC-2) and within the damage zone (LPC-1), are shown in Table 3 and Figures 10, 11. There is a clear difference in composition between the detrital muscovite and illite in most instances, with the former having a higher MR3 component (Figure 10). Furthermore, higher Fe and Ti and lower Si contents occur in the detrital muscovite (Figure 11; Table 3). However, some of the muscovite has a similar composition to illite, particularly the thin relict phases intimately associated with kaolinite aggregates. Bladed varieties of white mica may be remnants of detrital muscovite, as they have similar compositions.

DISCUSSION

Comparison with previous studies

The Hawkesbury Sandstone and the underlying Narrabeen Group have been the subject of petrographic and XRD studies (Loughnan 1963; Bayliss *et al.* 1965; Ward 1971; Bai & Keene 1996; Bai *et al.* 2001). The minerals recognised in the sublitharenites and litharenites hosting the faults, as well as their textural relationships, are similar to those reported by other authors.

Bai & Keene (1996) identified a paragenetic sequence in the sandstones of the Narrabeen Group involving minerals formed during early and late diagenetic stages. Of the early diagenetic minerals they recognised, only siderite and illite–smectite were observed in the present study.

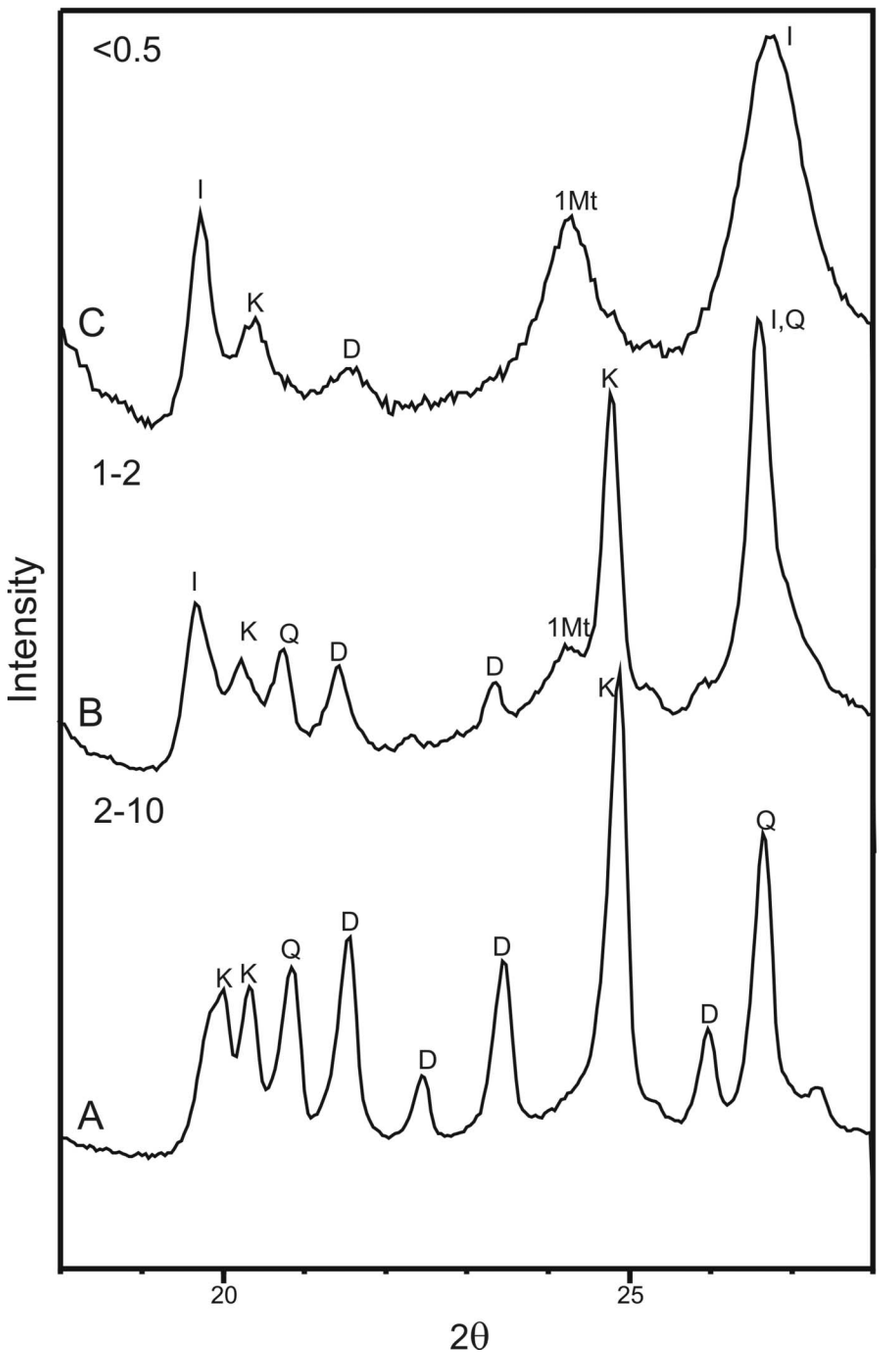

Figure 6 Air-dried XRD traces of LP3: A, 2–10 μm fraction; B, 1–2 μm fraction; C, <0.5 μm fraction. Symbols as in Figure 2; D, dickite.

The illite and kaolinite identified in this study are associated with quartz overgrowths, and are late diagenetic minerals according to the study of Bai & Keene (1996). However, if the assumption is made that quartz overgrowths, and the association kaolinite–illite, are the result of the thermal overprint (Och *et al.* 2009), the minerals considered by Bai & Keene (1996) to be of late diagenetic origin cannot be the result of burial. Evidence supporting a thermal origin is provided by the observation that quartz overgrowths are confined to an area in which mean maximum vitrinite reflectance (R_o) is equal to or greater than 0.8%, based on the data of Bai & Keene (1996; Appendix 1). Paleotemperatures are also higher in the Sydney area than further north in the Upper Permian sequences of the Newcastle area (Brown *et al.* 1996; Zwingmann *et al.* 2004). This increase in paleotemperature is not due to greater depth of burial, but is the result of high paleoheat flux during the Early Cretaceous (Faiz & Hutton 1993).

Conditions of formation

TEMPERATURE

Quantification of paleotemperatures in upper crustal rocks is difficult because of the lack of suitable geothermometers. However, some indication of paleotemperatures can be obtained from KI values, smectite

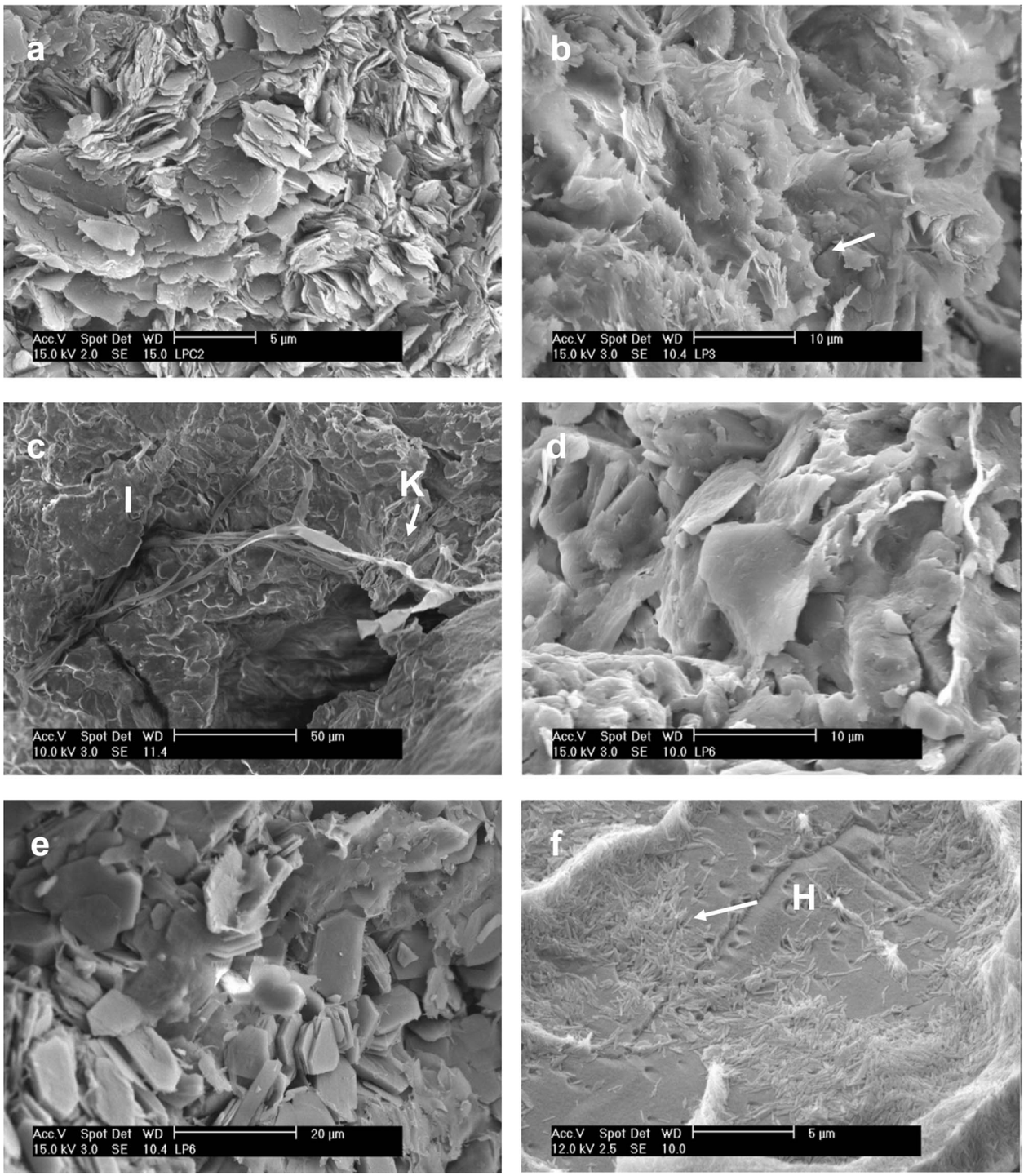

Figure 7 SEM photographs of clays. (a) Interlocking aggregate of interlocking, curviplanar, platy illite in sublitharenite outside damage zone of Luna Park Fault (LPC2). Note irregular boundaries of crystals. (b) Interlocking aggregate of platy illite showing filamentous illite at crystal boundaries (arrow): gouge from Luna Park Fault Zone (LP3). (c) Ribbon-like filamentous kaolinite (K; arrow) in a groundmass of quartz, kaolinite and illite (I): Heathcote Road Fault Zone (60–5). (d) Aggregate of curviplanar kaolinite with irregular boundaries (LP6). (e) Aggregate of blocky, pseudohexagonal kaolinite (LP6). (f) Clusters of tubular halloysite (arrow) in quartz showing etch pits (630). All samples are stored in the School of Environmental & Life Sciences, University of Newcastle.

content in illite/smectite, vitrinite reflectance (R_o) values obtained from coalified plant material, and fluid-inclusion analyses.

In the study area, illite and well-developed dickite books occur in gouges from the Luna Park Fault Zone and other fault zones, suggesting paleotemperatures

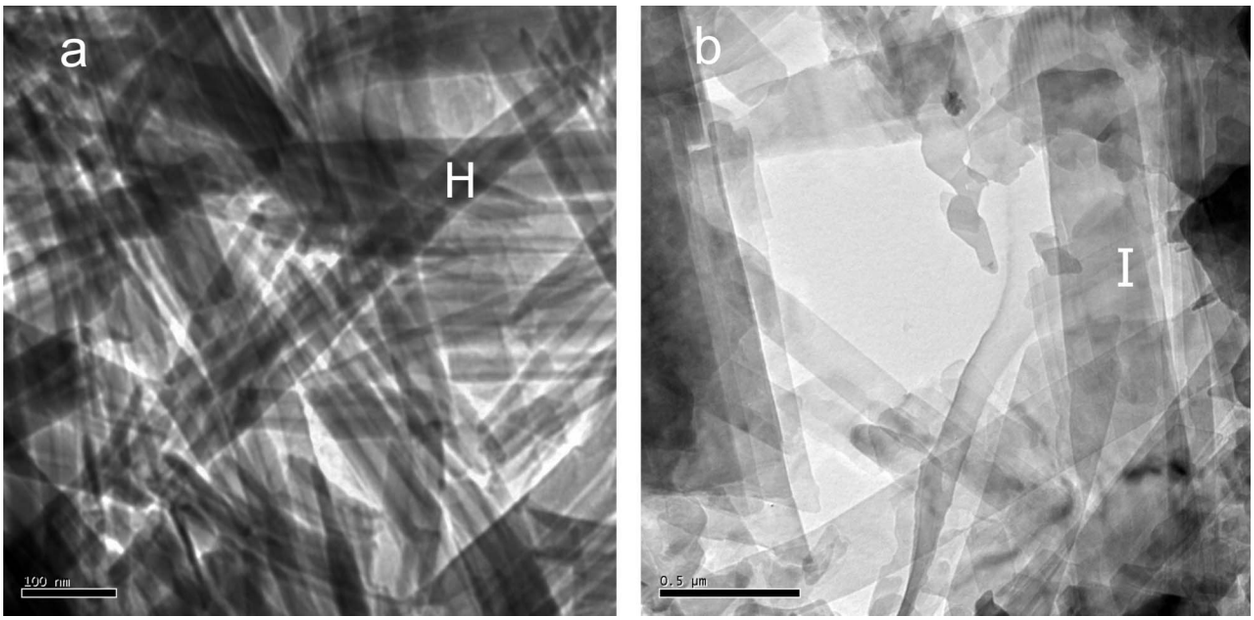

Figure 8 TEM photographs of clays. (a) Typical tubular morphology of halloysite (630). (b) Illite showing lath-like shape (599). All samples are stored in the School of Environmental & Life Sciences, University of Newcastle.

between 120 and 200°C based on $KI_{glyc.}$ values (0.54–0.71: Table 2), smectite content (Sme <10%: Table 1) (Yates & Rosenberg 1997; Merriman & Frey 1999) and the fact that dickite transforms from kaolinite at ~120°C (Ehrenberg *et al.* 1993). Similar temperatures of formation are recorded in the host-rocks of the Sydney region according to R_o studies of surface rocks [R_o=0.85–0.9% (Middleton & Schmidt 1982); R_o=1.0%, Lucas Heights (O'Sullivan *et al.* 1996)]. They indicate that the paleotemperatures varied from 130 to 143°C according to equations relating $R(v - r)$ (mean random vitrinite reflectance) and T proposed by Barker & Pawlewicz (1994). Paleotemperatures appear to have been slightly higher (175°C) in the Sydney region as R_o=1.3% (Brown *et al.* 1996). Fluid-inclusion studies of quartz overgrowths in sandstones from the Narrabeen Group taken from Liverpool 91 DDH in the Sydney region reveal similar paleotemperatures, ranging from 76 to >145°C (Bai *et al.* 2001). By contrast the presence of illite/smectite containing 30–38% Sme in the Heathcote Road Fault Zone suggests paleotemperatures of 100°C or less (Merriman & Frey 1999).

FLUID COMPOSITIONS AND PROCESSES

Mineral and textural relationships in the sublitharenites associated with the gouges provide an insight into the processes operating and compositions of fluids present when the mineral assemblages were formed. For example, the initial growth of illite and subsequently of kaolinite (Figure 2c) suggest that a fundamental change in fluid composition occurred because high a_{K+}/a_{H+} favours the growth of illite and low a_{K+}/a_{H+} the formation of kaolinite at the temperatures operating (Yates & Rosenberg 1997). The growth, in some samples, of kaolinite at the same time as the quartz overgrowths, suggests a_{Si4+} was high and a_{K+}/a_{H+} low. That conditions changed after the formation of these minerals is shown by the development of etch pits in quartz overgrowths and corrosion of crystal faces. These observations indicate that the fluid was not in equilibrium with quartz and a_{Si4+} must therefore have been low in the fluid. However, conditions were suitable for the growth of kaolinite, as the fluid with which it was in equilibrium corroded the overgrowths.

The triangular-shaped etch pits developed in detrital quartz and overgrowths are similar to those observed by Blum *et al.* (1990) and have been produced experimentally on quartz by Joshi & Kotru (1969) and Brantley *et al.* (1986). According to Brantley *et al.* (1986 and references therein), the development of such etch pits as well as their depth and number, are a function of the concentration of Si in the fluid phase, the time over which etching took place and the density of dislocations. Dislocation tangles cause preferential dissolution and drive diffusive mass transfer, and when strongly developed produce proportionally large numbers of etch pits (Brantley *et al.* 1986; Blum *et al.* 1990). Undersaturation of quartz in the fluids, leads to conditions suitable for the development of etch pits (Blum *et al.* 1990).

The occurrence of illite as filamentous aggregates commonly attached to platelets of illite is an indication of rapid crystallisation (Mullin 1961) controlled by nucleation kinetics (Güven 2001; Wilkinson & Haszeldine 2002; Meunier & Velde 2004). Formation of this type of illite is favoured by solutions with high fluid Al derived from the decomposition of thermally unstable aluminium oxalate complexes [$Al(COO)^{-2}$], with higher K^+/H^+ ratios than appropriate for the illite stability field in the phase diagram for the system K_2O–Al_2O_3–SiO_2–H_2O (Manning 2003). Further, illite growth in this form requires the host to have a high permeability and thus allow a high fluid influx (Moore & Reynolds 1997). Significantly, filamentous illite is observed in fault

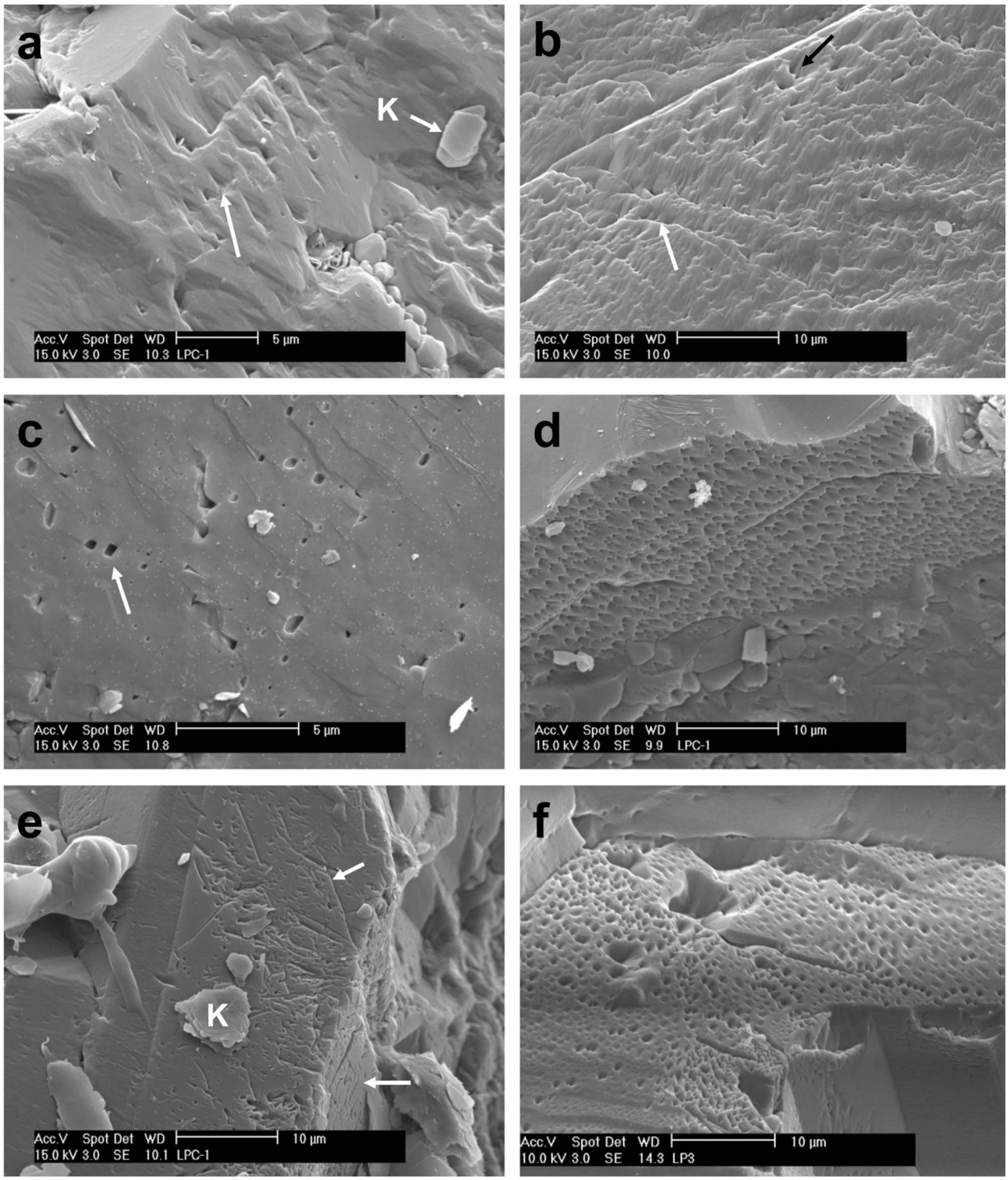

Figure 9 (a) Triangular etch pits in quartz (arrow). K, kaolinite (LPC-1). (b) Dense development of steeply plunging etch pits (black arrow), strongly oriented terraces in quartz (white arrow) LPC-1. (c) Widely scattered etch pits in quartz. Arrow shows rectangular etch pits: LPC-2. (d) Oblique view of well-developed, elongate etch pits in quartz overgrowth (LPC-3). (e) Different types of etch pits in overgrowth. Note different orientations of trench-like pits (arrow) and etch pits on a second face: sample (LPC-1) from damage zone. K, kaolinite. (f) Densely developed etch pits on face of quartz crystal in litharenite (LP3) from gouge. All samples are stored in the School of Environmental & Life Sciences, University of Newcastle.

gouges, indicating that the fault zones were channelways for major fluid flow.

The presence of kaolinite along the (001) cleavage of muscovite has been noted by a number of authors (Milliken 2003 and references therein). It indicates that this plane has been exploited by fluids responsible for the formation of kaolinite. Experimental studies have shown that muscovite has a high dissolution rate along

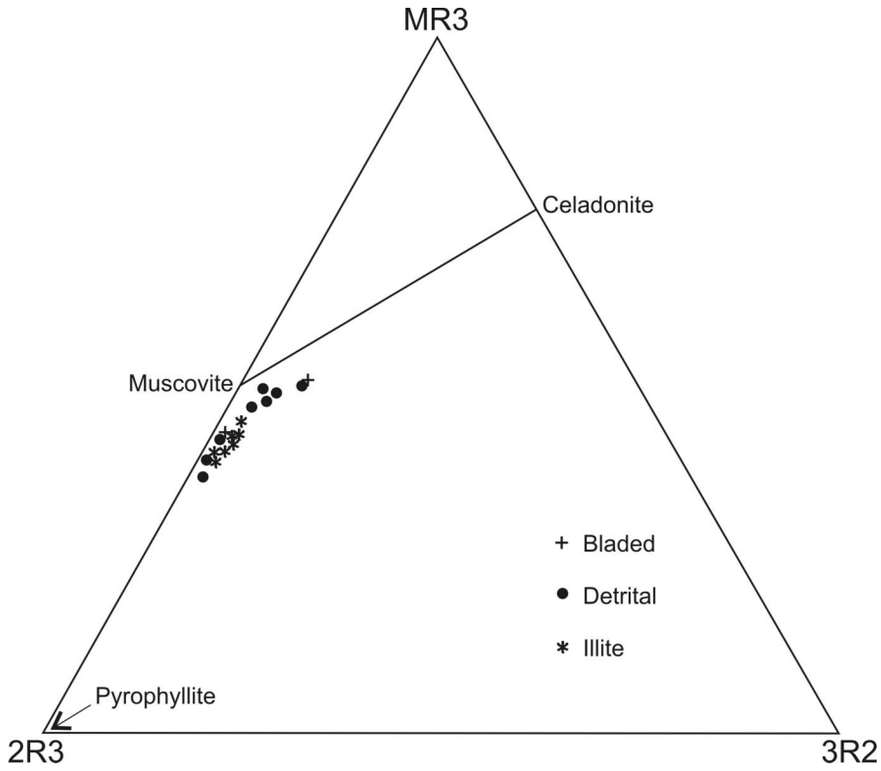

Figure 10 MR3–2R3–3R2 plot of illites and detrital muscovite compositions in host-rock adjacent to and within fault zones. MR3, [K + Na + 2Ca]; 2R3, [Al-(K + Na + 2Ca)]/2; 3R2, [Fe_2 + Mg + Mn]. Plot after Velde (1977).

the basal cleavage surfaces (Johnsonn *et al.* 1992). These surfaces are also ideal sites for nucleation of kaolinite when reacted with fluids supersaturated with this mineral (Nagy & Pevear 1993).

In summary, fluid compositions changed over time, with high a_{Si4+} present when the quartz overgrowths developed and high a_{K+}/a_{H+} in the fluid subsequently favouring the formation of illite. This was followed by precipitation of kaolinite from fluids with low a_{K+}/a_{H+} and a_{Si4+}. However, fluid compositions were different in some samples, as overgrowths and filamentous illite or kaolinite grew synchronously, implying that a_{Si4+} was high and a_{K+}/a_{H+} was very high or low, respectively.

REACTIONS AND SOURCE OF IONS RESPONSIBLE FOR THE CLAYS

Careful examination of slides of the host-rocks within the fault gouge does not reveal definitive textural evidence that would allow reactions to be proposed for the formation of the clays. In most instances, the elements required for their formation appear to have been released from the breakdown of detrital phases during the ingress of fluids into the fault zones (Table 4). However, in LPC1, a reaction front between detrital quartz and illite aggregates (Figure 2a) contains illite and Si-rich, K and Al-poor 'islands.' This association suggests the following reaction:

$$\underset{\text{kaolinite}}{2Al_2Si_2O_5(OH)_4} + \underset{\text{quartz}}{SiO_2} + K^+ = \underset{\text{illite}}{KAl_3O_{10}(OH)_2} + \underset{\text{Si-Al 'islands'}}{2Si(OH)_2 + Al^{3+}}$$

Derivation of K^+ and Al^{3+} required for the formation of illite in most samples appears to have been from detrital muscovite rather than K-feldspar, considered by many authors to be the main donor of K for illite (Meunier & Velde 2004 and references therein). The basis for this observation is that muscovite is a more common detrital phase in the present samples than K-feldspar, and also the common association of illite with muscovite. The minor occurrence of the association illite–anatase may indicate that at least some K^+ for illite has been derived from biotite. Further, the low proportions of Mg^{2+} and Fe^{2+} noted in the illite (Table 3) were most likely derived from biotite, opaque minerals and possibly siderite, mineral phases in the sublitharenites.

Formation of illite from smectite, as suggested by some authors, may explain the occurrence of illite between detrital quartz grains and overgrowths, since smectite commonly forms a coating around detrital grains during eodiagenesis (i.e. diagenetic modification due to shallow burial) (Worden & Morad 2003). However, illite that formed after the overgrowth event in these samples has not originated in this way because it does not show the cornflake morphology that is characteristic of the smectite–illite transformation (Pollastro 1985).

Although there are many possible sources of the Al^{3+} and Si^{4+} required for the formation of kaolinite (Table 4), the most likely candidates are feldspars and detrital muscovite since these are now replaced by kaolinite. Evidence for this is seen in Figure 2d, in which the total replacement of a mechanically strong mineral with a rectangular outline is represented. This was most likely to have been a feldspar, a mineral that is relatively uncommon in the Hawkesbury Sandstone (Bayliss *et al.* 1965). The observation that kaolinite aggregates appear to expand muscovite along (001) and almost totally replace it (Figure 2b) suggests that Al^{3+} and Si^{4+}

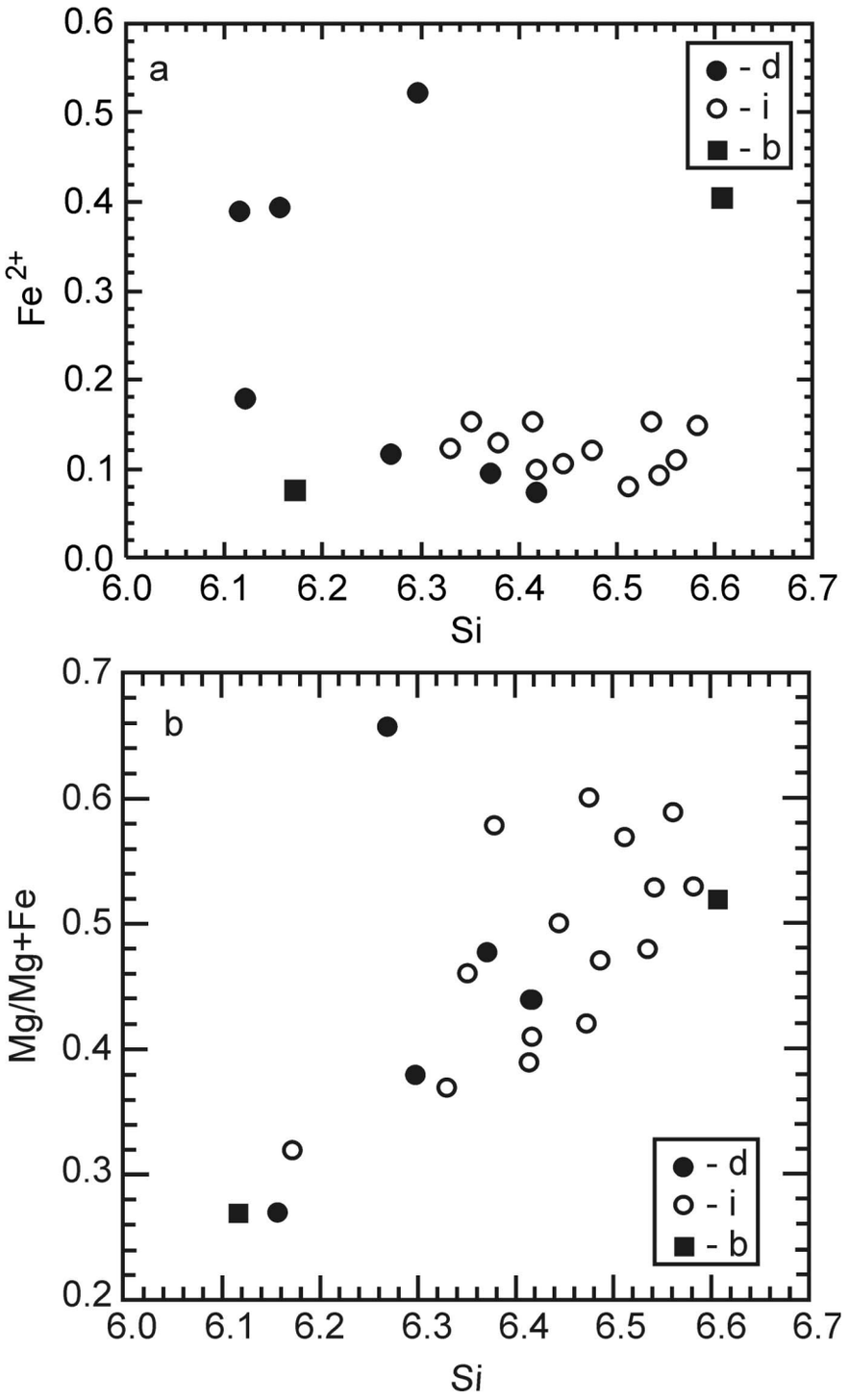

Figure 11 Fe^{2+} *vs* Si and Mg/(Mg+Fe) *vs* Si plots of illites and detrital muscovites in host-rocks adjacent to and within fault zones (see Table 3 for abbreviations).

released from the breakdown of mica contributed to kaolinite formation.

Si required for the formation of the quartz overgrowths most likely has come from the breakdown of detrital phases and as a result of pressure solution. Evidence for the latter is indicated by the presence of sutured contacts between quartz grains. However, to explain the substantial development of overgrowths observed in the sublitharenite fragments associated with gouge, an external source for the Si is more likely. In the fault zones, open-system conditions would have prevailed, and major influxes of fluid are likely to have occurred that transported the Si required for the overgrowth.

CONCLUSIONS

XRD, SEM and TEM studies indicate that the gouge in the north-northeast-striking faults in the Sydney region, is

Table 3 Representative analyses of illites and muscovites.

Sample	LPC-2							LP3		LPC-1			
Type	Detrital muscovite	Bladed muscovite	Illite	Bladed muscovite	Illite	Detrital muscovite	Illite	Illite	Detrital muscovite	Illite	Illite	Illite	Detrital muscovite
SiO_2	45.83	46.59	50.22	49.02	51.46	44.96	50.37	50.55	46.53	45.84	51.57	51.64	50.22
TiO_2	0.49	0.19	0.23	0.47	0.19	0.36	–	–	1.00	0.15	0.01	–	0.07
Al_2O_3	34.04	37.1	33.26	29.15	36.88	34.09	34.23	34.9	35.45	33	35.02	36.13	36.55
Cr_2O_3	0.11	–	0.01	0.09	0.06	0.04	0.06	–	0.11	0.04	0.02	–	–
FeO	3.51	0.69	1.35	3.58	1.46	3.42	1.42	0.86	1.62	1.12	1.02	0.75	0.68
MnO	0.07	0.03	–	–	–	–	0.08	0.01	–	–	0.04	0.06	0.02
MgO	0.74	0.18	0.84	2.18	0.53	0.7	0.75	0.55	0.89	0.88	0.83	0.55	0.3
CaO	–	0.18	0.27	–	0.59	0.08	0.07	0.01	0.09	0.33	0.27	0.16	0.42
Na_2O	0.6	1.52	0.19	0.18	0.21	0.61	0.15	0.04	0.64	0.08	0.05	0.07	0.13
K_2O	9.99	7.01	8.42	10.02	8.06	9.97	8.79	8.7	10.13	7.98	8.35	8.67	8.38
Total	95.38	93.49	94.79	94.69	99.44	94.23	95.92	95.62	96.46	89.42	97.18	98.03	96.77
Si	6.157	6.172	6.583	6.608	6.415	6.116	6.536	6.543	6.121	6.38	6.562	6.513	6.419
Al^{IV}	1.843	1.828	1.417	1.392	1.585	1.884	1.464	1.457	1.879	1.62	1.438	1.487	1.581
Sum T	8	8	8	8	8	8	8	8	8	8	8	8	8
Al^{VI}	3.542	3.96	3.717	3.235	3.829	3.577	3.767	3.863	3.613	3.789	3.81	3.879	3.92
Ti	0.05	0.019	0.023	0.048	0.018	0.037	–	–	0.099	0.016	0.001	–	0.007
Fe^{2+}	0.394	0.076	0.148	0.404	0.152	0.389	0.154	0.093	0.178	0.13	0.109	0.079	0.073
Cr	0.012	–	0.001	0.01	0.006	0.004	0.006	–	0.011	0.004	0.002	–	–
Mn	0.008	0.003	–	–	–	–	0.009	0.001	–	–	0.004	0.006	0.002
Mg	0.148	0.036	0.164	0.438	0.098	0.142	0.145	0.106	0.175	0.183	0.157	0.103	0.057
Ca	–	0.026	0.038	–	0.079	0.012	0.01	0.001	0.013	0.049	0.037	0.022	0.058
Na	0.156	0.39	0.048	0.047	0.051	0.161	0.038	0.01	0.163	0.022	0.012	0.017	0.032
K	1.712	1.185	1.408	1.723	1.282	1.73	1.455	1.437	1.7	1.417	1.356	1.395	1.366
Cations	14.022	13.695	13.547	13.905	13.515	14.052	13.584	13.511	13.952	13.61	13.488	13.501	13.515
Mg/(Fe + Mg)	0.27	0.32	0.53	0.52	0.39	0.27	0.48	0.53	0.5	0.58	0.59	0.57	0.44

Table 4 Source of ions for clays and overgrowth.

Detrital phase			Textural evidence
	[Si^{4+}]		Corroded quartz boundary
Quartz	→	illite	in contact with illite aggregates
	[K^+, Al^{3+}, Si^{4+}]		Replacement of muscovite by illite
Muscovite	→	illite + K^+	
	[Si^{4+}]		Corroded quartz boundary in contact with
Quartz	→	kaolinite	kaolinite aggregates
	[Si^{4+}, Al^{3+}]		Replacement of feldspar by kaolinite
Feldspar	→	kaolinite + K^+ +Na^++ Ca^{2+}	
	[K^+, Al^{3+}, Si^{4+}, Mg^{2+}, Fe^{2+}, Ti^{4+}]		Replacement of bioite by illite and anatase
Biotite?	→	illite + anatase + Fe^{2+} +Mg^{2+}	
	[K^+, Al^{3+}, Si^{4+}]		Replacement of felsic volcanic clasts by illite
Lithic clasts	→	illite	

made up of illite (<10% Sme) or less commonly illite–smectite (30–38% Sme) and kaolinite in varying proportions. Dickite and halloysite are minor phases. Host-rocks external to the fault zones are sublitharenites containing detrital quartz and less common muscovite. Illite and kaolinite fill pore spaces and replace detrital grains; siderite is commonly concentrated on bedding planes. By contrast, host-rocks in the damage zone contain less illite and kaolinite, and secondary quartz overgrowths are common.

KI show that the illites have formed under diagenetic conditions. SEM investigations reveal that the illite may exhibit a platy and filamentous morphology. The SEM studies also show that well-developed etch pits occur on the surface of the detrital quartz grains, as well as overgrowths in sublitharenite and single grains extracted from the gouges.

The overgrowths and assemblages developed in the host-rocks in the damage zones and gouges have formed at temperatures of ~120–150°C during a thermal event at 120 Ma related to emplacement of felsic magmas during the early stages of the rifting of East Gondwana (Och *et al.* 2009). High fluid/rock ratios existed in the fault zones during the formation of the mineral assemblages in the gouges and the host rocks from the damage zones.

Breakdown of detrital grains such as muscovite and quartz appears to have provided the ions required for the formation of the diagenetic minerals. Feldspar may also have contributed to their formation but there is only circumstantial evidence for this. The fluids present during these minerals changed in composition with time. Initially, during the growth of illite, a_{K+}/a_{H+} was high. With the incoming of kaolinite and associated development of etch pits in quartz, fluid composition changed and low a_{K+}/a_{H+} and a_{Si4+} prevailed.

ACKNOWLEDGEMENTS

We thank Bill Birch and Colin Ward for constructive comments that greatly improved the manuscript, Jiang Zhiyu for preparation of thin-sections and Jenny Zobec for assistance with XRD analyses. The cost of using the X-ray diffractometer and the Scanning Electron Microscope was covered by IGS funds.

REFERENCES

Bai G-P., Hamilton P. J., Eadington P. J. & Keene J. B. 2001. Fluid flow histories and diagenesis in Permo-Triassic sediments of the Sydney Basin, SE Australia—isotope and fluid inclusion constraints. *In*: Hill K. C. & Bernecker T. eds. *Eastern Australasian Basins Symposium, a refocussed energy perspective for the future,* pp. 251–260. Petroleum Exploration Society of Australia Special Publication.

Bai G-P. & Keene J. B. 1996. Petrology and diagenesis of Narrabeen Group sandstones, Sydney Basin, New South Wales. *Australian Journal of Earth Sciences* **43**, 525–538.

Bailey S. W. 1980. Structure of layer silicates. *In*: Brindley G. & Brown G. eds. *Crystal structures of clay minerals and their X-ray identification,* pp. 1–79. Mineralogical Society Monograph **5**.

Barker C. E. & Pawlewicz M. J. 1994. Calculation of vitrinite reflectance from thermal histories and peak temperatures. A comparison of methods. *In*: Mukhopadhyay P. K. & Dow W. G. eds. *Vitrinite reflectance as a maturity parameter—applications and limitations,* pp. 216–229. ACS Symposium Series **570**.

Bayliss P., Loughnan F. C. & Standard J. C. 1965. Dickite in the Hawkesbury Sandstone of the Sydney Basin, Australia. *American Mineralogist* **50**, 418–426.

Beaufort D., Cassagnabere S., Petit S., Lanson B., Berger G., Lacharpagne J. C. & Johansen H. 1998. Kaolinite-to-dickite reaction in sandstone reservoirs. *Clay Minerals* **33**, 297–316.

Blum A. E., Yund R. A. & Lasaga A. C. 1990. The effect of dislocation density on the dissolution rate of quartz. *Geochimica et Cosmochimica Acta* **54**, 283–297.

Brantley S. L., Crane S. R., Crerar D. A., Hellman R. & Stallard R. 1986. Dissolution at dislocation etch pits in quartz. *Geochimica et Cosmochimica Acta* **50**, 2349–2361.

Brown K., Casey D. A., Enever J. R., Facer R. A. & Wright K. 1996. New South Wales coal seam methane potential. *New South Wales Department of Mineral Resources Petroleum Bulletin* **2**.

Clark N. R. & Jones D. C. 1991. *Penrith 1:100 000 geological sheet 9030* (1st edition). Geological Survey of New South Wales, Sydney.

Drits V. A., Weber F., Salyn A. L. & Tsipursky S. L. 1993. X-ray identification of one-layer illite varieties: application of the study of illites around uranium deposits of Canada. *Clays and Clay Minerals* **41**, 389–398.

Ehrenberg S. N., Aargaard P., Wilson M. J., Fraser A. R. & Duthie D. M. L. 1993. Depth-dependent transformation of kaolinite to dickite in sandstones of the Norwegian shelf. *Clay Minerals* **28**, 325–352.

Faiz M. M. & Hutton A. C. 1993. Two kilometres of post-Permian sediment: did it exist? *In*: Diessel C. F. K. ed. *Proceedings of the 27th Newcastle Symposium on advances in the study of the Sydney Basin,* pp. 221–228. University of Newcastle, Newcastle.

Guggenheim S., Bain D. C., Bergaya F., Brigatti M. F., Drits V. A., Eberl D. D., Formoso M. L. L., Galán E., Merriman R. J., Peacor D. R., Stanjeck H. & Watanabe T. 2002. Report of the Association Internationale pour l'Etude des Argiles (AIPEA) Nomenclature Committee for 2001. Order, disorder and crystallinity in phyllosilicates and the use of the Crystallinity Index. *Clay Minerals* **37**, 389–393.

GÜVEN N. 2001. Mica structure and fibrous growth of illite. *Clays and Clay Minerals* **49**, 189–196.

HERBERT C. 1983. *Sydney 1:100 000 geological sheet 9130* (1st edition). Geological Survey of New South Wales, Sydney.

HIPPERT J. F. 1994. Direct observation of porosity in quartzite and phyllonite. *Neues Jahrbuch für Mineralogie Abhandlungen* **166**, 239–259.

JOHNSONN P. A., HOCHELLA M. F. JR, PARKS J. A. & BLUM A. E. 1992. Direct observation of muscovite basal plane dissolution and secondary phase formation. An XPS, LEED, and SFM study. *In*: Kharaka Y. K. & Maest A. S. eds. *Water–rock interaction,* pp. 159–162. Balkema, Rotterdam.

JOSHI M. S. & KOTRU P. N. 1969. Hydrothermal etching of matched fractured prism faces of natural quartz. *Soviet Physics: Crystallography* **14**, 427–428.

KISCH H. J. 1991. Illite crystallinity: recommendations on sample preparation, X-ray diffraction settings and interlaboratory standards. *Journal of Metamorphic Geology* **9**, 665–670.

KRUMM S. & BUGGISCH W. 1991. Sample preparation effects on illite crystallinity measurements, grain size gradation and particle orientation. *Journal of Metamorphic Geology* **9**, 671–678.

KÜBLER B. 1968. Evaluation quantitative de métamorphism par la cristallinité de l'illite. *Centre de Recherche de Pau, Societe National des Petroles d'Aquitaine Bulletin* **2**, 385–397.

LANSON B., BEAUFORT D., BERGER G., BARADAT J. & LACHARPAGNE J.-C. 1996. Illitization of diagenetic kaolinite-to-dickite conversion series: late-stage diagenesis of the lower Permian Rotliegend sandstone reservoir, offshore of the Netherlands. *Journal of Sedimentary Research* **66**, 501–518.

LANSON B., BEAUFORT D., BERGER G., BAUER A., CASSAGNBÈRE A. & MEUNIER A. 2002. Authigenic kaolin and illite minerals during burial diagenesis of sandstones: a review. *Clay Minerals* **37**, 1–22.

LOUGHNAN F. C. 1963. A petrographic study of a vertical section of the Narrabeen Group at Helensburgh, NSW. *Journal of the Geological Society of Australia* **10**, 177–192.

MANNING D. A. C. 2003. Experimental studies of clay mineral occurrence. *In*: Worden R. & Morad S. eds. *Clay mineral cements in sandstones,* pp. 177–190. International Association of Sedimentologists Special Publication **34**.

MAUGER A. J., CREASEY J. W. & HUNTINGTON J. F. 1984. *Sydney-SBFA 9D Sydney Basin fracture analysis series.* CSIRO Division of Mineral Physics, Sydney.

MERRIMAN R. J. & FREY M. 1999. Patterns of low-grade metamorphism in metapelitic rocks. *In*: Frey M. & Robinson M. eds. *Low-grade metamorphism,* pp. 61–107. Blackwell Science, Oxford.

MEUNIER A. & VELDE B. 2004. *Illite: origin, evolution and metamorphism.* Springer, Heidelberg.

MIDDLETON M. F. & SCHMIDT P. W. 1982. Paleothermometry of the Sydney Basin. *Journal of Geophysical Research* **87**, 5351–5359.

MILLIKEN K. L. 2003. Microscale distribution of kaolinite in Breathitt Formation sandstones (middle Pennsylvanian): implications for mass balance. *In*: Worden R. & Morad S. eds. *Clay mineral cements in sandstones,* pp. 343–360. International Association of Sedimentologists Special Publication **34**.

MOORE D. M. & REYNOLDS R. C. JR. 1997. *X-ray diffraction and the identification and analysis of clay minerals* (2nd edition). Oxford University Press, Oxford.

MULLIN J. W. 1961. *Crystallisation.* Butterworths, Guildford.

NAGY K. L. & PEVEAR D. R. 1993. Kinetics of muscovite dissolution and kaolinite precipitation onto muscovite at 80°C and pH 3.25. *Geological Society of America Abstract Program* **25**, A437.

OCH D. J., OFFLER R., ZWINGMANN H., BRAYBROOKE J. & GRAHAM I. T. 2009. Timing of brittle faulting and thermal events, Sydney region: association with the early stages of extension of East Gondwana. *Australian Journal of Earth Sciences* **56**.

O'SULLIVAN P. B., COYLE D. A., GLEADOW A. J. W. & KOHN B. P. 1996. Late Mesozoic to Early Cenozoic thermotectonic history of the Sydney Basin and the eastern Lachlan Fold Belt, Australia. *Geological Society of Australia Abstracts* **43**, 424–432.

POLLASTRO R. M. 1985. Mineralogical and morphological evidence for the formation of illite at the expense of illite/smectite. *Clays and Clay Minerals* **33**, 265–274.

ROBINSON D. 1981. Metamorphic rocks of an intermediate facies juxtaposed at the Start boundary, south-west England. *Geological Magazine* **118**, 297–301.

SIIVOLA J. & SCHMID R. 2007. List of mineral abbreviations. *In*: Fettes D. & Desmons J. eds. *Metamorphic rocks: a classification and glossary of terms,* pp. 126–204. Cambridge University Press, Cambridge.

STROUD W. J., SHERWIN L., ROY H. N. & BAKER C. J. 1985. *Wollongong—Port Hacking 1:100 000 geological sheet 9029 & 9129* (1st edition). Geological Survey of New South Wales, Sydney.

SUDO T., SHIMODA S., YOTSUMOTO H. & AITA S. 1981. *Electron micrographs of clay minerals* (Developments in Sedimentology **31**). Elsevier, Amsterdam.

VELDE B. 1977. *Clays and clay minerals in natural and synthetic systems.* Elsevier, Amsterdam.

WARD C. R. 1971. Mineralogical change as marker horizons for stratigraphic correlation in the Narrabeen Group of the Sydney Basin, NSW. *Proceedings of the Royal Society of New South Wales* **104**, 77–88.

WARR L. N. & RICE A. H. N. 1994. Interlaboratory standardisation and calibration of clay mineral crystallinity and crystallite size data. *Journal of Metamorphic Geology* **12**, 141–152.

WILKINSON M. & HASZELDINE R. S. 2002. Fibrous illite in oilfield sandstones—nucleation kinetic theory of growth. *Terra Nova* **14**, 56–60.

WORDEN R. & MORAD S. 2003. Clay minerals in sandstones: controls on formation, distribution and evolution. *In*: Worden R. & Morad S. eds. *Clay mineral cements in sandstones,* pp. 3–41. International Association of Sedimentologists Special Publication **34**.

YATES D. M. & ROSENBERG P. E. 1997. Formation and stability of end member illite: II. Solid equilibrium experiments at 100°C to 250°C and $P_{v,soln.}$. *Geochimica et Cosmochimica Acta* **61**, 3135–3144.

ZWINGMANN H., OFFLER R., WILSON T. & COX S. 204. K–Ar dating of fault gouge in the northern Sydney Basin, NSW, Australia—implications for the break up of Gondwana. *Journal of Structural Geology* **26**, 2285–2295.

Received 23 October 2007; accepted 7 April 2009